SCIENCE CHINA
Mathematics

• ARTICLES •

January 2019 Vol. 62 No. 1: 185–204
https://doi.org/10.1007/s11425-017-9315-9

A new piecewise quadratic approximation approach for L_0 norm minimization problem

Qian Li[1], Yanqin Bai[1,*], Changjun Yu[1] & Ya-xiang Yuan[2]

[1]*Department of Mathematics, Shanghai University, Shanghai* 200444, *China;*
[2]*Institute of Computational Mathematics and Scientific/Engineering Computing, Academy of Mathematics and Systems Science, Chinese Academy of Sciences, Beijing* 100190, *China*

*Email: liqian*15123329166@163.*com, yqbai@t.shu.edu.cn, yuchangjun*@126.*com, yyx@lsec.cc.ac.cn*

Received August 7, 2017; accepted May 2, 2018; published online December 4, 2018

Abstract In this paper, we consider the problem of finding sparse solutions for underdetermined systems of linear equations, which can be formulated as a class of L_0 norm minimization problem. By using the least absolute residual approximation, we propose a new piecewise quadratic function to approximate the L_0 norm. Then, we develop a piecewise quadratic approximation (PQA) model where the objective function is given by the summation of a smooth non-convex component and a non-smooth convex component. To solve the (PQA) model, we present an algorithm based on the idea of the iterative thresholding algorithm and derive the convergence and the convergence rate. Finally, we carry out a series of numerical experiments to demonstrate the performance of the proposed algorithm for (PQA). We also conduct a phase diagram analysis to further show the superiority of (PQA) over L_1 and $L_{1/2}$ regularizations.

Keywords sparse optimization, non-convex approximation, iterative thresholding algorithm

MSC(2010) 90C30, 90C59, 90C90

Citation: Li Q, Bai Y, Yu C, et al. A new piecewise quadratic approximation approach for L_0 norm minimization problem. Sci China Math, 2019, 62: 185–204, https://doi.org/10.1007/s11425-017-9315-9

1 Introduction

Sparsity problems have attracted considerable attention in both theoretical study and engineering practice in recent years, including variable selection [34], face recognition [41], image processing [7], matrix completion [8] and compressed sensing [17]. Finding sparse solutions for underdetermined systems of linear equations, as an important class of sparsity problems, is to recover a sparse vector $\boldsymbol{x} \in \mathbb{R}^n$ from the measurements:

$$\boldsymbol{b} = A\boldsymbol{x},$$

where $\boldsymbol{b} \in \mathbb{R}^m$ is an observation, and $A \in \mathbb{R}^{m\times n}$ $(m < n)$ is a measurement matrix of full row rank. Mathematically, this problem can be formulated as

$$(\mathrm{P}) \quad \min_{\boldsymbol{x}\in\mathbb{R}^n} \|\boldsymbol{x}\|_0 \quad \text{subject to} \quad \boldsymbol{b} = A\boldsymbol{x}, \tag{1.1}$$

* Corresponding author

where $\|\boldsymbol{x}\|_0$, known as the L_0 norm, is the number of nonzero components of $\boldsymbol{x}$. Instead of solving problem (P) directly, it is general to consider the following L_0 regularization problem:

$$\min_{\boldsymbol{x}\in\mathbb{R}^n}\{\|\boldsymbol{b}-A\boldsymbol{x}\|^2+\lambda\|\boldsymbol{x}\|_0\}, \tag{1.2}$$

where $\|\cdot\|$ denotes the Euclidean norm and $\lambda>0$ is a regularization parameter to balance the weights of two terms in the objective.

L_0 regularization problem is in general challenging to solve as it is NP-hard [29]. In order to overcome such difficulty, L_1 regularization has been proposed

$$\min_{\boldsymbol{x}\in\mathbb{R}^n}\{\|\boldsymbol{b}-A\boldsymbol{x}\|^2+\lambda\|\boldsymbol{x}\|_1\}, \tag{1.3}$$

where $\|\boldsymbol{x}\|_1=\sum_{i=1}^n|x_i|$ is the L_1 norm. It is well known that L_1 regularization is a convex optimization problem. Hence, there exist many exclusive and efficient algorithms, for example, the interior-point method [12], least angle regression [18], two-step iterative shrinkage algorithm (TwIST) [3], Nesterov's algorithm (NESTA) [2], augmented Lagrangian method (ALM) [42], soft thresholding algorithm (soft algorithm) [13, 16], and fast iterative shrinkage-thresholding algorithm (FISTA) [1]. Under certain circumstances, a solution of L_1 regularization is the solution of L_0 regularization (L_1/L_0 equivalence) [17]. However, L_1 regularization cannot guarantee a solution with desired sparsity in some case. There are some convex improvements on L_1 regularization, such as the weighted LASSO and the corrected LASSO [36].

Further consideration for solving the L_0 regularization problem is to solve the following L_q regularization problem:

$$\min_{\boldsymbol{x}\in\mathbb{R}^n}\{\|\boldsymbol{b}-A\boldsymbol{x}\|^2+\lambda\|\boldsymbol{x}\|_q^q\}, \tag{1.4}$$

where $\|\boldsymbol{x}\|_q=(\sum_{i=1}^n|x_i|^q)^{1/q}$, $0<q<1$, is the L_q quasi-norm. The L_q regularization leads to a non-convex, non-smooth, and nonlipschitz optimization problem. There are two types of algorithms for solving L_q regularization, the iterative reweighted algorithm [14, 26] and the iterative thresholding algorithm [23,45]. Nevertheless, how to choose an appropriate q to yield the best result is also a problem. Recently, this issue has been studied in [11, 33, 37, 38]. In particular, the special importance of $L_{1/2}$ regularization is highlighted [39, 40]. By developing a thresholding representation theory, an iterative half thresholding algorithm (half algorithm) [38] has been proposed for finding a fast solution to the $L_{1/2}$ regularization. The convergence result of the half algorithm has been given in [44].

Moreover, other non-convex approximations of the L_0 norm have been investigated, including smoothly clipped absolute deviation [19], log-sum penalty [10], minimax concave penalty [46] and L_{1-2} ($\|\boldsymbol{x}\|_1-\|\boldsymbol{x}\|$) minimization [43]. These approximations can be solved by four classes of algorithms, including the half-quadratic algorithm [21, 22], the iterative reweighted algorithm [10, 14, 24, 26], the difference of convex functions algorithm [20, 47], and the iterative thresholding algorithm [23, 45]. Among these algorithms, the iterative thresholding algorithm is mostly used, since it is easy to implement and has almost the least computational complexity for large scale problems [32].

In this paper, to solve the L_0 norm minimization problem, we first propose a new piecewise quadratic function to approximate the L_0 norm, and then develop a piecewise quadratic approximation (PQA) model. The objective function of (PQA) contains a smooth non-convex term and a non-smooth convex term. Then, we present an iterative algorithm for solving (PQA) based on the iterative thresholding algorithm [1, 23] and prove that it converges to an ϵ stationary point within $\mathcal{O}(1/\epsilon)$ iterations. Finally, we provide a series of numerical experiments to demonstrate the performance of the proposed algorithm for solving (PQA). We also conduct a phase diagram analysis to further show the superiority of (PQA) over L_1 and $L_{1/2}$ regularizations.

The rest of this paper is organized as follows. In Section 2, a new piecewise quadratic approximation is proposed. We develop an iterative algorithm for solving (PQA) and establish its convergence properties in Section 3. In Section 4, we carry out a series of numerical experiments, including signal recovery and image recovery, to show the performance of the iterative algorithm for solving (PQA). We finally conduct

a phase diagram analysis in Section 5 to further demonstrate the superiority of (PQA) over L_1 and $L_{1/2}$ regularizations. We conclude this paper in Section 6.

2 The piecewise quadratic approximation

2.1 The new approximation for L_0 norm

It is well known that L_0 regularization is generally difficult to solve since it is NP-hard [29]. In the past decade, various approximations to the L_0 norm have been proposed, including $\|\boldsymbol{x}\|_1$ and $\|\boldsymbol{x}\|_q^q$ $(0<q<1)$. In this section, we will derive a new approximation for the L_0 norm.

Without loss of generality, we first investigate the approximation for the L_0 norm over $[-\boldsymbol{e},\boldsymbol{e}]$, $\boldsymbol{e}=(1,1,\ldots,1)^{\mathrm{T}}$. Consider the set

$$\mathcal{S}=[-\boldsymbol{e},\boldsymbol{e}]=\{\boldsymbol{x}=(x_1,x_2,\ldots,x_n)^{\mathrm{T}}:x_i\in[-1,1],i=1,2,\ldots,n\}.$$

There exist a series of $a_{ij}\in\{0,1\},i=1,2,\ldots,n,j=1,2,\ldots,2^n$, such that $\{S_j\}$, where

$$S_j=\{\boldsymbol{x}\in\mathcal{S}:x_i\in[-a_{ij},1-a_{ij}],i=1,2,\ldots,n\},\quad j=1,2,\ldots,2^n,$$

is a partition of $\mathcal{S}$ satisfying $\mathrm{int}(S_j)\neq\emptyset,\ j=1,2,\ldots,2^n$, $\mathrm{int}(S_i)\cap\mathrm{int}(S_j)=\emptyset$ for $i\neq j$, and

$$\mathcal{S}=S_1\cup S_2\cup\cdots\cup S_{2^n}.$$

For illustration, we consider the two-dimensional case where $\mathcal{S}=\{\boldsymbol{x}=(x_1,x_2)^{\mathrm{T}}:x_i\in[-1,1],i=1,2\}$. We have the following partition for $\mathcal{S}$:

$$S_1=\{\boldsymbol{x}:x_1\in[0,1],x_2\in[0,1]\},\quad S_2=\{\boldsymbol{x}:x_1\in[-1,0],x_2\in[0,1]\},$$
$$S_3=\{\boldsymbol{x}:x_1\in[-1,0],x_2\in[-1,0]\},\quad S_4=\{\boldsymbol{x}:x_1\in[0,1],x_2\in[-1,0]\}.$$

By the definition of $\|\boldsymbol{x}\|_0$, $\|\boldsymbol{x}\|_1$ and $\|\boldsymbol{x}\|_q^q$ $(0<q<1)$, we observe that they share the following properties:

(i) The function values of them are equal at the vertex of each S_j, $j=1,2,\ldots,2^n$.

(ii) They are concave on each of S_j, $j=1,2,\ldots,2^n$.

(iii) They are monotonically decreasing on $[-1,0)$ and monotonically increasing on $(0,1]$ with respect to each of the component $x_i,i=1,2,\ldots,n$.

Motivated by these properties, we approximate $\|\boldsymbol{x}\|_0$ by the following piecewise quadratic function:

$$P(\boldsymbol{x})=\begin{cases}\boldsymbol{x}^{\mathrm{T}}H^1\boldsymbol{x}+(\boldsymbol{h}^1)^{\mathrm{T}}\boldsymbol{x}, & \boldsymbol{x}\in S_1,\\ \quad\vdots & \quad\vdots\\ \boldsymbol{x}^{\mathrm{T}}H^l\boldsymbol{x}+(\boldsymbol{h}^l)^{\mathrm{T}}\boldsymbol{x}, & \boldsymbol{x}\in S_l,\\ \quad\vdots & \quad\vdots\\ \boldsymbol{x}^{\mathrm{T}}H^{2^n}\boldsymbol{x}+(\boldsymbol{h}^{2^n})^{\mathrm{T}}\boldsymbol{x}, & \boldsymbol{x}\in S_{2^n},\end{cases}$$

where $\boldsymbol{x}=(x_1,x_2,\ldots,x_n)^{\mathrm{T}}$, $l=1,2,\ldots,2^n$, $(H_{ij}^l)\in\mathbb{R}^{n\times n}$ and $\boldsymbol{h}^l=(h_1^l,h_2^l,\ldots,h_n^l)^{\mathrm{T}}$. To ensure the proposed piecewise quadratic function shares the above properties and moreover, to achieve a good approximation, it is essential to find appropriate H^l and $\boldsymbol{h}^l$. We want the area between $\|\boldsymbol{x}\|_0$ and $P(\boldsymbol{x})$ over $[-\boldsymbol{e},\boldsymbol{e}]$ minimized. These help us to determine H^l and $\boldsymbol{h}^l$, $l=1,2,\ldots,2^n$.

By definition, $P(\boldsymbol{x})$ is symmetric over each of the hyperplane $x_i=0,i=1,2,\ldots,n$. Thus, we only need to compute H^1 and $\boldsymbol{h}^1$ in

$$\boldsymbol{x}^{\mathrm{T}}H^1\boldsymbol{x}+(\boldsymbol{h}^1)^{\mathrm{T}}\boldsymbol{x},\quad \boldsymbol{x}\in S_1.$$

We set $S_1=[\boldsymbol{0},\boldsymbol{e}]$, where $\boldsymbol{0}=(0,0,\ldots,0)^{\mathrm{T}}$. For simplicity, we denote H^1 and $\boldsymbol{h}^1$ as H and $\boldsymbol{h}$, respectively.

By Property (i), the value of $\boldsymbol{x}^{\mathrm{T}}H\boldsymbol{x}+\boldsymbol{h}^{\mathrm{T}}\boldsymbol{x}$ should be equal to $\|\boldsymbol{x}\|_0$ at the vertex of $[\boldsymbol{0},\boldsymbol{e}]$. Set $\boldsymbol{x}=\boldsymbol{e}_i$, where $\boldsymbol{e}_i=(0,\ldots,1,\ldots,0)^{\mathrm{T}},\ i=1,2,\ldots,n$. From $\boldsymbol{e}_i^{\mathrm{T}}H\boldsymbol{e}_i+\boldsymbol{h}^{\mathrm{T}}\boldsymbol{e}_i=\|\boldsymbol{e}_i\|_0$, we get

$$H_{ii}+h_i=1. \tag{2.1}$$

Then, we set $\boldsymbol{x}=\boldsymbol{e}_i+\boldsymbol{e}_j, i\neq j, i,j=1,2,\ldots,n$, with $\|\boldsymbol{x}\|_0=2$. From $(\boldsymbol{e}_i+\boldsymbol{e}_j)^{\mathrm{T}}H(\boldsymbol{e}_i+\boldsymbol{e}_j)+\boldsymbol{h}^{\mathrm{T}}(\boldsymbol{e}_i+\boldsymbol{e}_j)=2$, we have

$$H_{ii}+2H_{ij}+H_{jj}+h_i+h_j=2. \tag{2.2}$$

Combining (2.1) and (2.2), we obtain

$$H_{ij}=0,\quad i\neq j, \tag{2.3}$$

and hence H is a diagonal matrix.

By Property (ii), $P(\boldsymbol{x})$ should be concave on S_l, $l=1,2,\ldots,2^n$, and hence

$$H_{ii}\leqslant 0,\quad i=1,2,\ldots,n. \tag{2.4}$$

By Property (iii), it is natural to assume that $\boldsymbol{x}^{\mathrm{T}}H\boldsymbol{x}+\boldsymbol{h}^{\mathrm{T}}\boldsymbol{x}$ is monotonically increasing with respect to each of x_i over $[0,1]$. Therefore, we have

$$2H_{ii}x_i+h_i\geqslant 0,\quad \forall\, x_i\in[0,1],\quad i=1,2,\ldots,n. \tag{2.5}$$

Combining (2.1), (2.4) and (2.5), we have

$$-1\leqslant H_{ii}\leqslant 0,\quad 1\leqslant h_i\leqslant 2,\quad i=1,2,\ldots,n. \tag{2.6}$$

Finally, the area between $\|\boldsymbol{x}\|_0$ and $\boldsymbol{x}^{\mathrm{T}}H\boldsymbol{x}+\boldsymbol{h}^{\mathrm{T}}\boldsymbol{x}$ over $[\boldsymbol{0},\boldsymbol{e}]$ is minimized

$$\min_{H,\boldsymbol{h}} S=\int_0^1\cdots\int_0^1 |\|\boldsymbol{x}\|_0-\boldsymbol{x}^{\mathrm{T}}H\boldsymbol{x}-\boldsymbol{h}^{\mathrm{T}}\boldsymbol{x}|dx_1\cdots dx_n \tag{2.7}$$

with constraints (2.1), (2.3) and (2.6) to obtain H and $\boldsymbol{h}$. By (2.1), (2.3) and (2.6), we have

$$\boldsymbol{x}^{\mathrm{T}}H\boldsymbol{x}+\boldsymbol{h}^{\mathrm{T}}\boldsymbol{x}=\sum_{i=1}^{n}(H_{ii}x_i^2+h_ix_i)\leqslant\|\boldsymbol{x}\|_0,\quad \boldsymbol{x}\in[\boldsymbol{0},\boldsymbol{e}]. \tag{2.8}$$

Furthermore, (2.7) can be reformulated as the following problem:

$$\min_{\boldsymbol{h}}\int_0^1\cdots\int_0^1\|\boldsymbol{x}\|_0dx_1\cdots dx_n-\int_0^1\cdots\int_0^1\sum_{i=1}^{n}[(x_i-x_i^2)h_i+x_i^2]dx_1\cdots dx_n \tag{2.9}$$

with the constraint (2.6). Combining (2.1), (2.6) and (2.9), we obtain $H_{ii}=-1, h_i=2, i=1,2,\ldots,n$.

Therefore,

$$\boldsymbol{x}^{\mathrm{T}}H\boldsymbol{x}+\boldsymbol{h}^{\mathrm{T}}\boldsymbol{x}=-\boldsymbol{x}^{\mathrm{T}}\boldsymbol{x}+2\boldsymbol{e}^{\mathrm{T}}\boldsymbol{x}.$$

Remark 2.1. For the training points $\boldsymbol{x}^j\in[\boldsymbol{0},\boldsymbol{e}]$, we consider the following least absolute residual approximation problem:

$$\min_{H,\boldsymbol{h}}\sum_j(\|\boldsymbol{x}^j\|_0-(\boldsymbol{x}^j)^{\mathrm{T}}H\boldsymbol{x}^j-\boldsymbol{h}^{\mathrm{T}}\boldsymbol{x}^j). \tag{2.10}$$

This model is minimizing the sum of absolute residuals between $\|\boldsymbol{x}\|_0$ and $\boldsymbol{x}^{\mathrm{T}}H\boldsymbol{x}+\boldsymbol{h}^{\mathrm{T}}\boldsymbol{x}$ at the training point $\boldsymbol{x}^j$. Instead of solving (2.7), solving (2.10) can obtain the same H and $\boldsymbol{h}$ as above.

By symmetry, we can finally obtain the piecewise quadratic approximation function

$$P(\boldsymbol{x})=-\boldsymbol{x}^{\mathrm{T}}\boldsymbol{x}+2\|\boldsymbol{x}\|_1,\quad \boldsymbol{x}\in[-\boldsymbol{e},\boldsymbol{e}].$$

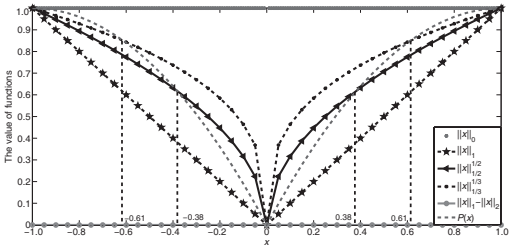

(a) $-1 \leqslant x \leqslant 1$

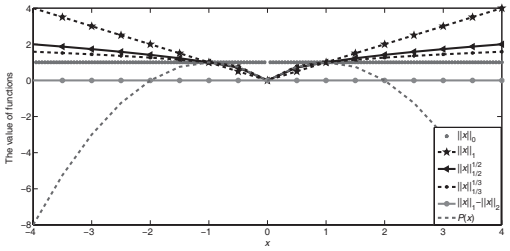

(b) $-4 \leqslant x \leqslant 4$

Figure 1 Various approximations for the one-dimensional case

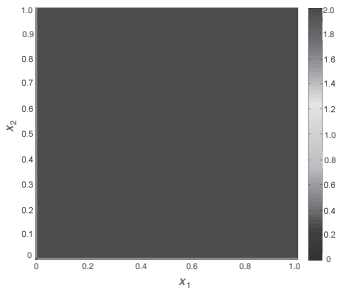

(a) $\|\boldsymbol{x}\|_0$

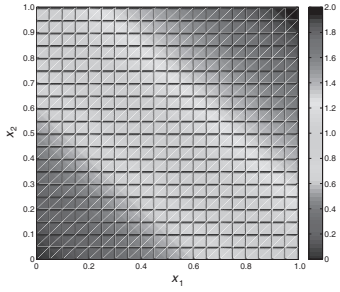

(b) $\|\boldsymbol{x}\|_1$

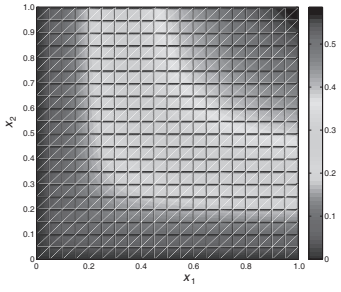

(c) $\|\boldsymbol{x}\|_1 - \|\boldsymbol{x}\|$

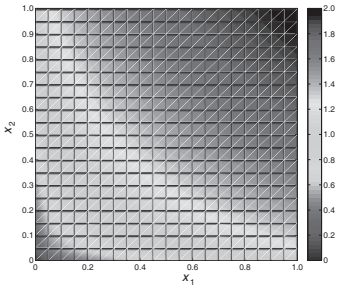

(d) $\|\boldsymbol{x}\|_{1/2}^{1/2}$

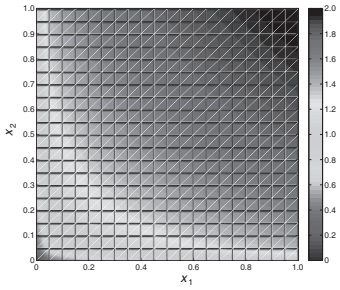

(e) $\|\boldsymbol{x}\|_{1/3}^{1/3}$

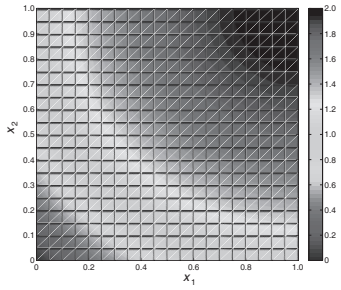

(f) $-\boldsymbol{x}^{\mathrm{T}}\boldsymbol{x} + 2\|\boldsymbol{x}\|_1$

Figure 2 Various approximations for the two-dimensional case

Remark 2.2. As above, we obtain the piecewise quadratic function to approximate $\|\boldsymbol{x}\|_0$ over $[-\boldsymbol{e}, \boldsymbol{e}]$. Then, we extend the domain of $P(\boldsymbol{x})$ to $\mathbb{R}^n$, i.e., $P(\boldsymbol{x}) = -\boldsymbol{x}^{\mathrm{T}}\boldsymbol{x} + 2\|\boldsymbol{x}\|_1$, $\boldsymbol{x} \in \mathbb{R}^n$. However, outside $[-\boldsymbol{e}, \boldsymbol{e}]$, $\|\boldsymbol{x}\|_0$ cannot be well approximated by $P(\boldsymbol{x})$ (see Figure 1(b)). As a result, when we use $P(\boldsymbol{x})$ to develop the piecewise quadratic approximation model, we will introduce a scaling parameter t to restrict all the iterations of $\boldsymbol{x}$ in $[-\boldsymbol{e}, \boldsymbol{e}]$.

In what follows, we shall illustrate the approximation effects of $\|\boldsymbol{x}\|_1$, $\|\boldsymbol{x}\|_{1/2}^{1/2}$, $\|\boldsymbol{x}\|_{1/3}^{1/3}$, $\|\boldsymbol{x}\|_1 - \|\boldsymbol{x}\|$ and $P(\boldsymbol{x})$ for one-dimensional and two-dimensional cases, respectively.

For the one-dimensional case, the figures of $\|x\|_0$, $\|x\|_1$, $\|x\|_{1/2}^{1/2}$, $\|x\|_{1/3}^{1/3}$, $\|x\|_1 - \|x\|$ and $P(x)$ are plotted in Figure 1(a). From the geometric point of view, $P(x)$ is superior to $\|x\|_1$ on approximating the L_0 norm when $|x| \leqslant 1$. More specifically, when $0.38 \leqslant |x| \leqslant 1$, $P(x)$ gives a better approximation to $\|x\|_0$, as compared with $\|x\|_{1/2}^{1/2}$. $P(x)$ gives a better approximation to $\|x\|_0$ than $\|x\|_{1/3}^{1/3}$ when $0.61 \leqslant |x| \leqslant 1$. For $\|x\|_1 - \|x\|$, it remains zero for the one-dimensional case and hence is not a good approximation for $\|x\|_0$.

In Figure 1(b), we can see that $\|x\|_0$ cannot be well approximated by $\|x\|_1$, $\|x\|_{1/2}^{1/2}$, $\|x\|_{1/3}^{1/3}$ and $P(x)$ when $|x| > 1$. This is because when $|x| > 1$, $P(x)$ is decreasing, while $\|x\|_1$, $\|x\|_{1/2}^{1/2}$ and $\|x\|_{1/3}^{1/3}$ are increasing. Thus, it is necessary to consider the approximation within $[-\boldsymbol{e}, \boldsymbol{e}]$.

Figure 2 shows the figures of $\|\boldsymbol{x}\|_0$, $\|\boldsymbol{x}\|_1$, $\|\boldsymbol{x}\|_{1/2}^{1/2}$, $\|\boldsymbol{x}\|_{1/3}^{1/3}$, $\|\boldsymbol{x}\|_1 - \|\boldsymbol{x}\|$ and $P(\boldsymbol{x})$ for the two-dimensional

case ($\mathbf{0} \leqslant \boldsymbol{x} \leqslant \boldsymbol{e}$). We observe from Figure 2 that $P(\boldsymbol{x})$ is still superior to $\|\boldsymbol{x}\|_1$ and $\|\boldsymbol{x}\|_1 - \|\boldsymbol{x}\|$ on approximating $\|\boldsymbol{x}\|_0$. Although $\|\boldsymbol{x}\|_{1/2}^{1/2}$ and $\|\boldsymbol{x}\|_{1/3}^{1/3}$ are superior to $P(\boldsymbol{x})$ in the neighborhood of $(0,0)$, $P(\boldsymbol{x})$ gives a better approximation in the neighborhood of $(1,1)$ when compared with $\|\boldsymbol{x}\|_{1/2}^{1/2}$ and $\|\boldsymbol{x}\|_{1/3}^{1/3}$.

2.2 The piecewise quadratic approximation of L_0 norm minimization problem

We now consider the piecewise quadratic approximation of L_0 norm minimization problem:

$$\begin{aligned} \text{(PQA)} \qquad \min \quad & -\left\|\frac{\boldsymbol{x}}{t}\right\|^2 + 2\left\|\frac{\boldsymbol{x}}{t}\right\|_1 \\ \text{subject to} \quad & \boldsymbol{b} = A\boldsymbol{x}, \end{aligned}$$

where $t > 1$ is a scaling parameter. The (PQA) model can be viewed as an approximation of a scaled L_0 norm minimization problem

$$\text{(SP)} \quad \min_{\boldsymbol{x}\in\mathbb{R}^n} \left\|\frac{\boldsymbol{x}}{t}\right\|_0 \quad \text{subject to} \quad \boldsymbol{b} = A\boldsymbol{x}, \tag{2.11}$$

where the problem (SP) is equivalent to the problem (P). This is because $\|\boldsymbol{x}\|_0 = \|\boldsymbol{x}/t\|_0$, when $t > 1$.

Remark 2.3. In the (PQA) model, the objective value is generally unbounded. However, by introducing a scaling parameter t, it becomes possible to restrict all the iterations of $\boldsymbol{x}$ within a box in $\mathbb{R}^n$. In Section 3, we will derive a parameter-setting strategy for t, such that all iterative points $\boldsymbol{x}^k$ generated by the proposed algorithm satisfy

$$\boldsymbol{x}^k \in [-t\boldsymbol{e}, t\boldsymbol{e}], \quad k \geqslant 0,$$

and consequently, the objective values of (PQA) at $\boldsymbol{x}^k$ ($k \geqslant 0$) are bounded from below. Moreover, the boundedness of the iterative points is an indispensable condition to ensure the convergence result of the proposed iterative algorithm for solving the problem (PQA).

2.3 A simple example

In this subsection, we give an example where $\|\boldsymbol{x}\|_1$, $\|\boldsymbol{x}\|_{1/2}^{1/2}$, $\|\boldsymbol{x}\|_{1/3}^{1/3}$ and $\|\boldsymbol{x}\|_1 - \|\boldsymbol{x}\|$ fail to find the sparsest solution, while $P(\boldsymbol{x})$ succeeds. Consider the following example:

$$A = \begin{pmatrix} 5 & 10 & 10 & 10 \\ -5 & 20 & 0 & 10 \\ -3 & 10 & 0 & 0 \end{pmatrix}, \quad \boldsymbol{b} = \begin{pmatrix} 15 \\ 15 \\ 7 \end{pmatrix}.$$

The basic feasible solutions of $\boldsymbol{b} = A\boldsymbol{x}$ are

$$\boldsymbol{x} = \begin{pmatrix} 0 \\ 7/10 \\ 7/10 \\ 1/10 \end{pmatrix} + c \begin{pmatrix} -10 \\ -3 \\ 7 \\ 1 \end{pmatrix}, \quad c \in \mathbb{R}. \tag{2.12}$$

It is obvious that all the possible objective values of (P) in this example are $\{0,1,2,3,4\}$. $(0,0,0,0)^{\mathrm{T}}$ is not the feasible solution of (P), so the minimum of (P) cannot be 0. From (2.12), there is no such c that $\boldsymbol{x}$ only has one non-zero component. So the minimum of (P) cannot be 1. When $c = -0.1$, $\boldsymbol{x}^* = (1,1,0,0)^{\mathrm{T}}$ is the unique optimal solution of (P). Thus the minimum of (P) is 2.

It is not difficult to verify that the unique optimal solution of

$$\min\{\|\boldsymbol{x}\|_1 \,|\, \boldsymbol{b} = A\boldsymbol{x}\}$$

is $\overline{\boldsymbol{x}} = (0, 0.7, 0.7, 0.1)^{\mathrm{T}}$, and the optimal value is 1.5. Next, we use $P(\boldsymbol{x})$ to relax the L_0 norm. We set $-1/10 \leqslant c \leqslant 3/70$ which ensures $|\boldsymbol{x}| \leqslant \boldsymbol{e}$. The optimal solution of

$$\min\{-\boldsymbol{x}^{\mathrm{T}}\boldsymbol{x} + 2\|\boldsymbol{x}\|_1 \,|\, \boldsymbol{b} = A\boldsymbol{x}\}$$

may be obtained at $\boldsymbol{x}$ when $c = -1/10, 3/70$ or 0. It is easy to verify that when $c = -1/10$, we obtain the optimal solution $\boldsymbol{x}^* = (1, 1, 0, 0)^{\mathrm{T}}$, which is the sparsest solution.

However, the optimal solution of

$$\min\{\|\boldsymbol{x}\|_1 - \|\boldsymbol{x}\| \,|\, \boldsymbol{b} = A\boldsymbol{x}\}$$

is not $\boldsymbol{x}^*$, because $\|\overline{\boldsymbol{x}}\|_1 - \|\overline{\boldsymbol{x}}\| < \|\boldsymbol{x}^*\|_1 - \|\boldsymbol{x}^*\|$. Moreover, $\|\overline{\boldsymbol{x}}\|_{1/2}^{1/2} < \|\boldsymbol{x}^*\|_{1/2}^{1/2}$ and $\|\overline{\boldsymbol{x}}\|_{1/3}^{1/3} < \|\boldsymbol{x}^*\|_{1/3}^{1/3}$, so $\boldsymbol{x}^*$ is not the optimal solution of

$$\min\{\|\boldsymbol{x}\|_{1/2}^{1/2} \,|\, \boldsymbol{b} = A\boldsymbol{x}\}, \quad \min\{\|\boldsymbol{x}\|_{1/3}^{1/3} \,|\, \boldsymbol{b} = A\boldsymbol{x}\}.$$

Therefore, the non-convex approximations $\|\boldsymbol{x}\|_1 - \|\boldsymbol{x}\|$, $\|\boldsymbol{x}\|_{1/2}^{1/2}$ and $\|\boldsymbol{x}\|_{1/3}^{1/3}$ cannot obtain the sparsest solution in this example, while $P(\boldsymbol{x})$ can. Of course, one could construct other examples in which $\|\boldsymbol{x}\|_1 - \|\boldsymbol{x}\|$, $\|\boldsymbol{x}\|_{1/2}^{1/2}$ and $\|\boldsymbol{x}\|_{1/3}^{1/3}$ approximations would perform better than the piecewise quadratic approximation.

The objective function of (PQA) is given by the summation of a smooth non-convex component and a non-smooth convex component, whereas the objective function of the L_{1-2} problem is given by the summation of a non-smooth convex component and a non-smooth non-convex component, which is generally more difficult to solve. Actually, $\|\boldsymbol{x}\|_q^q, 0 < q < 1$ can provide a better approximation to $\|\boldsymbol{x}\|_0$, when the value of q is smaller. However, when $1/2 \leqslant q < 1$, the $L_{1/2}$ regularization always yields the best sparse solution and when $0 < q \leqslant 1/2$, the performance of the regularizations takes no significant difference [39]. In numerical experiments, $L_{1/2}$ regularization will be taken as a representative of L_q regularizations to compare with the (PQA) model, which can be solved by the half algorithm efficiently.

In the next sections, we will present an iterative algorithm for solving the (PQA) model and provide a series of experiments and applications to further demonstrate the performance of the (PQA) model.

3 Computational approach

Denote $f(\boldsymbol{x}) = -\|\boldsymbol{x}/t\|^2$ and

$$g(\boldsymbol{x}) = \begin{cases} 2\left\|\dfrac{\boldsymbol{x}}{t}\right\|_1, & \boldsymbol{x} \in X, \\ +\infty, & \boldsymbol{x} \notin X, \end{cases}$$

where $X = \{\boldsymbol{x} \,|\, \boldsymbol{b} = A\boldsymbol{x}\}$. Obviously, $f : \mathbb{R}^n \to \mathbb{R}$ is a smooth non-convex function of the type $\mathcal{C}_{L_f}^{1,1}(\mathbb{R}^n)$, i.e., continuously differentiable with Lipschitz continuous gradient

$$\|\nabla f(\boldsymbol{x}) - \nabla f(\boldsymbol{y})\| \leqslant L_f\|\boldsymbol{x} - \boldsymbol{y}\|, \quad \forall\, \boldsymbol{x}, \boldsymbol{y} \in \mathbb{R}^n,$$

where $L_f > 0$ is the Lipschitz constant of ∇f. In addition, $g : \mathbb{R}^n \to \mathbb{R}$ is a non-smooth convex function.

In this section, we first develop an iterative algorithm to solve the following general formulation which includes the problem (PQA) as a special case:

$$\min_{\boldsymbol{x} \in \mathbb{R}^n} F(\boldsymbol{x}) \equiv f(\boldsymbol{x}) + g(\boldsymbol{x}). \tag{3.1}$$

To continue, we assume that the following conditions hold:

1. f is a smooth non-convex function of the type $\mathcal{C}_{L_f}^{1,1}(\mathbb{R}^n)$.
2. g is a proper closed convex function which is possibly non-smooth.

3.1 The iterative algorithm

In accordance with the basic idea of the iterative thresholding algorithm [1,23], we consider the following quadratic approximation of $F(\boldsymbol{x})$ at a given point $\boldsymbol{y}$:

$$Q_{L_f}(\boldsymbol{x},\boldsymbol{y}) := f(\boldsymbol{y}) + \langle \boldsymbol{x}-\boldsymbol{y}, \nabla f(\boldsymbol{y})\rangle + \frac{L_f}{2}\|\boldsymbol{x}-\boldsymbol{y}\|^2 + g(\boldsymbol{x}).$$

This formulation admits a unique minimizer

$$P_{L_f}(\boldsymbol{y}) := \arg\min\{Q_{L_f}(\boldsymbol{x},\boldsymbol{y}) : \boldsymbol{x}\in\mathbb{R}^n\},$$

which can be rewritten as

$$P_{L_f}(\boldsymbol{y}) := \arg\min_{\boldsymbol{x}}\left\{g(\boldsymbol{x}) + \frac{L_f}{2}\left\|\boldsymbol{x}-\left(\boldsymbol{y}-\frac{1}{L_f}\nabla f(\boldsymbol{y})\right)\right\|^2\right\}.$$

The operator $P_{L_f}(\boldsymbol{y})$ mentioned in the above formula is actually the proximal mapping [28,31] of g at the point $\boldsymbol{y}-(1/L_f)\nabla f(\boldsymbol{y})$, where the proximal mapping is defined as

$$\mathrm{prox}_{cg}(\boldsymbol{u}) = \arg\min_{\boldsymbol{x}}\left\{g(\boldsymbol{x}) + \frac{1}{2c}\|\boldsymbol{x}-\boldsymbol{u}\|^2\right\}.$$

Based on the above results and the iterative thresholding algorithm for convex problems [1], we are now ready to describe the basic iteration of the iterative algorithm for solving the problem (3.1).

Algorithm 1 The iterative algorithm (IA)

1: **Input:** L_f: The Lipschitz constant of ∇f;
2: **Step 0:** Take $\boldsymbol{x}^0\in\mathbb{R}^n$;
3: **Step k:** ($k\geqslant 1$) Compute

$$\boldsymbol{x}^k = \mathrm{prox}_{\frac{1}{L_f}g}\left(\boldsymbol{x}^{k-1}-\frac{1}{L_f}\nabla f(\boldsymbol{x}^{k-1})\right). \tag{3.2}$$

Note that (3.2) can also be written as $\boldsymbol{x}^k = P_{L_f}(\boldsymbol{x}^{k-1})$. In the next subsection, we shall derive the convergence and the convergence rate of Algorithm 1.

3.2 Convergence analysis

Before establishing the convergence of Algorithm 1, we shall present a key result (see Lemma 3.3 below) that will be crucial for the convergence analysis. First, we recall the fundamental property for a smooth function in the class $\mathcal{C}^{1,1}_{L_f}(\mathbb{R}^n)$ (see [30, Lemma 1.2.3]).

Lemma 3.1. *Let $f:\mathbb{R}^n\to\mathbb{R}$ be a continuously differentiable function with Lipschitz continuous gradient and Lipschitz constant L_f. Then, for any $\boldsymbol{x},\boldsymbol{y}\in\mathbb{R}^n$, we have*

$$-\frac{L_f}{2}\|\boldsymbol{x}-\boldsymbol{y}\|^2 \leqslant f(\boldsymbol{x}) - f(\boldsymbol{y}) - \langle \boldsymbol{x}-\boldsymbol{y}, \nabla f(\boldsymbol{y})\rangle \leqslant \frac{L_f}{2}\|\boldsymbol{x}-\boldsymbol{y}\|^2.$$

We also need the following result which characterizes the optimality of $P_{L_f}(\cdot)$ (see [1, Lemma 2.2]).

Lemma 3.2. *For any $\boldsymbol{y}\in\mathbb{R}^n$, one has $\boldsymbol{z} = P_{L_f}(\boldsymbol{y})$ if and only if there exists $\gamma(\boldsymbol{y})\in\partial g(\boldsymbol{z})$, the subdifferential of $g(\cdot)$, such that*

$$\nabla f(\boldsymbol{y}) + L_f(\boldsymbol{z}-\boldsymbol{y}) + \gamma(\boldsymbol{y}) = 0.$$

We are now ready to give the promised key result as follows.

Lemma 3.3. *Let $\boldsymbol{y}\in\mathbb{R}^n$. Then for any $\boldsymbol{x}\in\mathbb{R}^n$,*

$$F(\boldsymbol{x}) - F(P_{L_f}(\boldsymbol{y})) \geqslant \frac{L_f}{2}\|P_{L_f}(\boldsymbol{y})-\boldsymbol{x}\|^2 - L_f\|\boldsymbol{x}-\boldsymbol{y}\|^2.$$

Proof. From Lemma 3.1, we have

$$F(P_{L_f}(\boldsymbol{y})) \leqslant Q(P_{L_f}(\boldsymbol{y}), \boldsymbol{y}).$$

Thus,

$$F(\boldsymbol{x}) - F(P_{L_f}(\boldsymbol{y})) \geqslant F(\boldsymbol{x}) - Q(P_{L_f}(\boldsymbol{y}), \boldsymbol{y}). \tag{3.3}$$

Since Lemma 3.1 and $g(\boldsymbol{x})$ is convex, we have

$$\begin{aligned} f(\boldsymbol{x}) &\geqslant f(\boldsymbol{y}) + \langle \boldsymbol{x} - \boldsymbol{y}, \nabla f(\boldsymbol{y})\rangle - \frac{L_f}{2}\|\boldsymbol{x} - \boldsymbol{y}\|^2, \\ g(\boldsymbol{x}) &\geqslant g(P_{L_f}(\boldsymbol{y})) + \langle \boldsymbol{x} - P_{L_f}(\boldsymbol{y}), \gamma(\boldsymbol{y})\rangle. \end{aligned}$$

Summing the two inequalities up yields

$$F(\boldsymbol{x}) \geqslant f(\boldsymbol{y}) + g(P_{L_f}(\boldsymbol{y})) + \langle \boldsymbol{x} - \boldsymbol{y}, \nabla f(\boldsymbol{y})\rangle + \langle \boldsymbol{x} - P_{L_f}(\boldsymbol{y}), \gamma(\boldsymbol{y})\rangle - \frac{L_f}{2}\|\boldsymbol{x} - \boldsymbol{y}\|^2. \tag{3.4}$$

On the other hand, by the definition of $P_{L_f}(\boldsymbol{y})$, one has

$$Q(P_{L_f}(\boldsymbol{y}), \boldsymbol{y}) = f(\boldsymbol{y}) + \langle P_{L_f}(\boldsymbol{y}) - \boldsymbol{y}, \nabla f(\boldsymbol{y})\rangle + \frac{L_f}{2}\|P_{L_f}(\boldsymbol{y}) - \boldsymbol{y}\|^2 + g(P_{L_f}(\boldsymbol{y})). \tag{3.5}$$

Therefore, substituting (3.4) and (3.5) into (3.3) gives

$$\begin{aligned} F(\boldsymbol{x}) - F(P_{L_f}(\boldsymbol{y})) &\geqslant \langle \boldsymbol{x} - P_{L_f}(\boldsymbol{y}), \nabla f(\boldsymbol{y}) + \gamma(\boldsymbol{y})\rangle - \frac{L_f}{2}\|\boldsymbol{x} - \boldsymbol{y}\|^2 - \frac{L_f}{2}\|P_{L_f}(\boldsymbol{y}) - \boldsymbol{y}\|^2 \\ &= L_f\langle \boldsymbol{x} - P_{L_f}(\boldsymbol{y}), \boldsymbol{y} - P_{L_f}(\boldsymbol{y})\rangle - \frac{L_f}{2}\|\boldsymbol{x} - \boldsymbol{y}\|^2 - \frac{L_f}{2}\|P_{L_f}(\boldsymbol{y}) - \boldsymbol{y}\|^2 \\ &= \frac{L_f}{2}\|P_{L_f}(\boldsymbol{y}) - \boldsymbol{x}\|^2 - L_f\|\boldsymbol{x} - \boldsymbol{y}\|^2, \end{aligned}$$

where the first equality above comes from Lemma 3.2. □

The following lemma shows that the sequence $\{\boldsymbol{x}^k\}$ generated by Algorithm 1 converges to a stationary point of (3.1) as $\|L_f(\boldsymbol{x}^k - \boldsymbol{x}^{k-1})\|^2$ decreases. It is served as a stopping criterion for Algorithm 1.

Lemma 3.4. *Let $\{\boldsymbol{x}^k\}$ be the sequence generated by Algorithm 1. If $\|L_f(\boldsymbol{x}^k - \boldsymbol{x}^{k-1})\|^2 \leqslant \epsilon$ after k iterations, then there exists $\gamma(\boldsymbol{x}^{k-1}) \in \partial g(\boldsymbol{x}^k)$, such that*

$$\|\nabla f(\boldsymbol{x}^k) + \gamma(\boldsymbol{x}^{k-1})\|^2 \leqslant 4\epsilon.$$

Proof. Since $\{\boldsymbol{x}^k\}$ is the sequence generated by Algorithm 1, we have $\boldsymbol{x}^k = P_{L_f}(\boldsymbol{x}^{k-1})$. By Lemma 3.2 and the first-order optimality condition, we have

$$-\nabla f(\boldsymbol{x}^{k-1}) - L_f(\boldsymbol{x}^k - \boldsymbol{x}^{k-1}) \in \partial g(\boldsymbol{x}^k).$$

Let $\gamma(\boldsymbol{x}^{k-1}) = -\nabla f(\boldsymbol{x}^{k-1}) - L_f(\boldsymbol{x}^k - \boldsymbol{x}^{k-1})$. We have

$$\|\nabla f(\boldsymbol{x}^k) + \gamma(\boldsymbol{x}^{k-1})\|^2 \leqslant 4\|L_f(\boldsymbol{x}^k - \boldsymbol{x}^{k-1})\|^2 \leqslant 4\epsilon,$$

where the first inequality is taken from

$$\|\nabla f(\boldsymbol{x}^k) + \gamma(\boldsymbol{x}^{k-1})\| \leqslant \|\nabla f(\boldsymbol{x}^k) - \nabla f(\boldsymbol{x}^{k-1})\| + L_f\|\boldsymbol{x}^k - \boldsymbol{x}^{k-1}\| \leqslant 2L_f\|\boldsymbol{x}^k - \boldsymbol{x}^{k-1}\|.$$

This completes the proof. □

In what follows, we discuss the convergence and the convergence rate of Algorithm 1.

Theorem 3.5. *Let $\{\boldsymbol{x}^k\}$ be the sequence generated by Algorithm 1. Assume that $\{\boldsymbol{x}^k\}$ is bounded. Then the following statements hold*:

(i) $\sum_{k=0}^{\infty}\|\boldsymbol{x}^{k+1} - \boldsymbol{x}^k\|^2 < \infty$.

(ii) *Any accumulation point of $\{\boldsymbol{x}^k\}$ is a stationary point of F.*

Proof. Invoking Lemma 3.3 with $\boldsymbol{x} = \boldsymbol{y} = \boldsymbol{x}^k$, we obtain

$$F(\boldsymbol{x}^k) - F(\boldsymbol{x}^{k+1}) \geqslant \frac{L_f}{2}\|\boldsymbol{x}^{k+1} - \boldsymbol{x}^k\|^2, \quad \forall\, k \geqslant 0, \tag{3.6}$$

which implies that the sequence $\{F(\boldsymbol{x}^k)\}$ is monotonically decreasing. Summing both sides of (3.6) from 0 to N, we have

$$\sum_{k=0}^{N} \frac{L_f}{2}\|\boldsymbol{x}^{k+1} - \boldsymbol{x}^k\|^2 \leqslant F(\boldsymbol{x}^0) - F(\boldsymbol{x}^{N+1}). \tag{3.7}$$

Since $\{\boldsymbol{x}^k\}$ is bounded, together with the fact that $\{F(\boldsymbol{x}^k)\}$ is monotonically decreasing, $\{F(\boldsymbol{x}^k)\}$ is convergent. Let $N \to \infty$ in (3.7). We conclude

$$\sum_{k=0}^{\infty} \frac{L_f}{2}\|\boldsymbol{x}^{k+1} - \boldsymbol{x}^k\|^2 < \infty.$$

So this proves (i).

We now prove (ii). Let $\boldsymbol{x}^*$ be an accumulation point of the sequence $\{\boldsymbol{x}^k\}$. Then, there exists a subsequence $\{\boldsymbol{x}^{k_i}\}$ such that $\lim_{i\to\infty} \boldsymbol{x}^{k_i} = \boldsymbol{x}^*$. Using Lemma 3.2, we obtain

$$-L_f(\boldsymbol{x}^{k_i+1} - \boldsymbol{x}^{k_i}) \in \nabla f(\boldsymbol{x}^{k_i}) + \partial g(\boldsymbol{x}^{k_i+1}). \tag{3.8}$$

Invoking $\|\boldsymbol{x}^{k_i+1} - \boldsymbol{x}^{k_i}\| \to 0$ from (i), together with the continuity of ∇f and the closeness of ∂g [35], passing to the limit in (3.8), we have

$$0 \in \nabla f(\boldsymbol{x}^*) + \partial g(\boldsymbol{x}^*).$$

It means that $\boldsymbol{x}^*$ is a stationary point of F.

This completes the proof. □

Based on Theorem 3.5, we know that $\|\boldsymbol{x}^{k+1} - \boldsymbol{x}^k\|^2$ is a quantity to measure the convergence of the sequence $\{\boldsymbol{x}^k\}$ to a stationary point of F. In the following theorem, we present the convergence rate in terms of $\|\boldsymbol{x}^{k+1} - \boldsymbol{x}^k\|^2$.

Theorem 3.6. *Let $\{\boldsymbol{x}^k\}$ be the sequence generated by Algorithm* 1. *Assume that $\{\boldsymbol{x}^k\}$ is bounded. Then for any $N \geqslant 1$, there exists a constant M such that*

$$\min_{k=0,\ldots,N-1} \|L_f(\boldsymbol{x}^{k+1} - \boldsymbol{x}^k)\|^2 \leqslant \frac{2(N+1)ML_f^2}{N(N-1)}. \tag{3.9}$$

Proof. Invoking Lemma 3.3 with $\boldsymbol{y} = \boldsymbol{x}^k$, $\boldsymbol{x} = \boldsymbol{x}^*$, where $\boldsymbol{x}^*$ is an accumulation point of $\{\boldsymbol{x}^k\}$, we obtain

$$F(\boldsymbol{x}^*) - F(\boldsymbol{x}^{k+1}) \geqslant \frac{L_f}{2}\|\boldsymbol{x}^{k+1} - \boldsymbol{x}^*\|^2 - L_f\|\boldsymbol{x}^k - \boldsymbol{x}^*\|^2. \tag{3.10}$$

Since $\{F(\boldsymbol{x}^k)\}$ is monotonically decreasing and $\{\boldsymbol{x}^k\}$ is bounded, we have $\lim_{k\to\infty} F(\boldsymbol{x}^k) = F(\boldsymbol{x}^*)$ and $F(\boldsymbol{x}^k) \geqslant F(\boldsymbol{x}^*), k \geqslant 0$. Summing the inequality (3.10) over $k = 0, 1, \ldots, N-1$ gives

$$0 \geqslant NF(\boldsymbol{x}^*) - \sum_{k=0}^{N-1} F(\boldsymbol{x}^{k+1}) \geqslant \frac{L_f}{2}\|\boldsymbol{x}^N - \boldsymbol{x}^*\|^2 - \frac{L_f}{2}\|\boldsymbol{x}^0 - \boldsymbol{x}^*\|^2 - \frac{L_f}{2}\sum_{k=0}^{N-1}\|\boldsymbol{x}^k - \boldsymbol{x}^*\|^2. \tag{3.11}$$

Invoking Lemma 3.3 one more time with $\boldsymbol{x} = \boldsymbol{y} = \boldsymbol{x}^k$ yields

$$F(\boldsymbol{x}^k) - F(\boldsymbol{x}^{k+1}) \geqslant \frac{L_f}{2}\|\boldsymbol{x}^{k+1} - \boldsymbol{x}^k\|^2.$$

Multiplying the last inequality by k and summing over $k = 0, 1, \ldots, N-1$, we obtain

$$\sum_{k=0}^{N-1}(kF(\boldsymbol{x}^k) - kF(\boldsymbol{x}^{k+1})) \geqslant \frac{L_f}{2}\sum_{k=0}^{N-1} k\|\boldsymbol{x}^{k+1} - \boldsymbol{x}^k\|^2,$$

which can be simplified to

$$-NF(\boldsymbol{x}^N)+\sum_{k=0}^{N-1}(F(\boldsymbol{x}^{k+1}))\geqslant\frac{L_f}{2}\sum_{k=0}^{N-1}k\|\boldsymbol{x}^{k+1}-\boldsymbol{x}^k\|^2. \tag{3.12}$$

Adding (3.11) and (3.12), we get

$$\begin{aligned}0&\geqslant NF(\boldsymbol{x}^*)-NF(\boldsymbol{x}^N)\\&\geqslant\frac{L_f}{2}\|\boldsymbol{x}^N-\boldsymbol{x}^*\|^2-\frac{L_f}{2}\|\boldsymbol{x}^0-\boldsymbol{x}^*\|^2-\frac{L_f}{2}\sum_{k=0}^{N-1}\|\boldsymbol{x}^k-\boldsymbol{x}^*\|^2+\frac{L_f}{2}\sum_{k=0}^{N-1}k\|\boldsymbol{x}^{k+1}-\boldsymbol{x}^k\|^2.\end{aligned} \tag{3.13}$$

By the assumption that $\{\boldsymbol{x}^k\}$ is bounded, there exists a constant M such that

$$\|\boldsymbol{x}^k-\boldsymbol{x}^*\|^2\leqslant M,\quad\forall\,k\geqslant 0,$$

and hence

$$\sum_{k=0}^{N-1}k\|\boldsymbol{x}^{k+1}-\boldsymbol{x}^k\|^2\leqslant(N+1)M.$$

Then (3.9) follows. This completes the proof. □

It follows from (3.9) that after running Algorithm 1 for at most $\mathcal{O}(1/\epsilon)$ iterations, we can obtain a stationary point $\boldsymbol{x}^k$ satisfying $\|L_f(\boldsymbol{x}^k-\boldsymbol{x}^{k-1})\|^2\leqslant\epsilon$, i.e., $\|\nabla f(\boldsymbol{x}^k)+\gamma(\boldsymbol{x}^{k-1})\|^2\leqslant 4\epsilon$, $\gamma(\boldsymbol{x}^{k-1})\in\partial g(\boldsymbol{x}^k)$.

Remark 3.7. Some algorithms related to our proposed algorithm are the generalized gradient projection algorithm [6, 25], the general iterative shrinkage and thresholding algorithm [23], and the iterative jumping thresholding algorithm [45]. Compared with the assumptions on the problem formulation, we can find that the optimization problem considered in this paper is different from the problems studied in [6, 23, 25, 45] (where they need the objective function values to be bounded from below). However, there are many non-convex optimization problems whose objective function values are not bounded from below, while the iterative points generated by the algorithm may be bounded.

The key of the convergence result for Algorithm 1 to solve the problem (PQA) relies on the boundedness of the iterative points, which will be proved in the following subsections.

3.3 Solving the subproblem

When we use Algorithm 1 to solve the problem (PQA), it is necessary to solve a convex subproblem of the following form at each iteration:

$$\min_{\boldsymbol{x}}\left\{g(\boldsymbol{x})+\frac{L_f}{2}\left\|\boldsymbol{x}-\left(\boldsymbol{x}^{k-1}-\frac{1}{L_f}\nabla f(\boldsymbol{x}^{k-1})\right)\right\|^2\right\}.$$

This problem can be simplified as

$$\begin{aligned}\min\quad&\frac{1}{t^2}\|\boldsymbol{x}-2\boldsymbol{x}^{k-1}\|^2+\frac{2}{t}\|\boldsymbol{x}\|_1\\\text{subject to}\quad&\boldsymbol{b}=A\boldsymbol{x},\end{aligned} \tag{3.14}$$

where $L_f=2/t^2$. Let

$$\psi(\boldsymbol{x},\boldsymbol{x}^{k-1})=\frac{1}{t^2}\|\boldsymbol{x}-2\boldsymbol{x}^{k-1}\|^2+\frac{2}{t}\|\boldsymbol{x}\|_1.$$

The subproblem (3.14) is a strongly convex problem, whose Lagrange dual problem is unconstrained, convex and differentiable.

In this subsection, we present the Lagrange dual problem of (3.14), and introduce Nesterov's accelerated gradient algorithm [30] to solve the dual problem.

Since $\|\boldsymbol{x}\|_1 = \max\{\boldsymbol{x}^{\mathrm{T}}\boldsymbol{z} : \boldsymbol{z} \in \mathbb{R}^n, \|\boldsymbol{z}\|_\infty \leqslant 1\}$ [27], the dual problem of (3.14) can be obtained as

$$\begin{aligned}\min_{\boldsymbol{x}}\{\psi(\boldsymbol{x}, \boldsymbol{x}^{k-1}) : A\boldsymbol{x} = \boldsymbol{b}\} &= \min_{\boldsymbol{x}}\max_{\boldsymbol{y}}\left\{\frac{1}{t^2}\|\boldsymbol{x} - 2\boldsymbol{x}^{k-1}\|^2 + \frac{2}{t}\|\boldsymbol{x}\|_1 - \boldsymbol{y}^{\mathrm{T}}(A\boldsymbol{x} - \boldsymbol{b})\right\}\\ &= \min_{\boldsymbol{x}}\max_{\boldsymbol{y},\boldsymbol{z}}\left\{\frac{1}{t^2}\|\boldsymbol{x} - 2\boldsymbol{x}^{k-1}\|^2 + \frac{2}{t}\boldsymbol{x}^{\mathrm{T}}\boldsymbol{z} - \boldsymbol{y}^{\mathrm{T}}A\boldsymbol{x} + \boldsymbol{y}^{\mathrm{T}}\boldsymbol{b} : \|\boldsymbol{z}\|_\infty \leqslant 1\right\}\\ &= \max_{\boldsymbol{y},\boldsymbol{z}}\left\{\min_{\boldsymbol{x}}\frac{1}{t^2}\|\boldsymbol{x} - 2\boldsymbol{x}^{k-1}\|^2 + \frac{2}{t}\boldsymbol{x}^{\mathrm{T}}\boldsymbol{z} - \boldsymbol{y}^{\mathrm{T}}A\boldsymbol{x} + \boldsymbol{y}^{\mathrm{T}}\boldsymbol{b} : \|\boldsymbol{z}\|_\infty \leqslant 1\right\}\\ &= -\min_{\boldsymbol{y},\boldsymbol{z}}\left\{-\boldsymbol{b}^{\mathrm{T}}\boldsymbol{y} + \left\|\frac{t}{2}A^{\mathrm{T}}\boldsymbol{y} + \frac{2}{t}\boldsymbol{x}^{k-1} - \boldsymbol{z}\right\|^2 - \frac{4}{t^2}\|\boldsymbol{x}^{k-1}\|^2 : \|\boldsymbol{z}\|_\infty \leqslant 1\right\},\end{aligned}$$

where the last equality comes from the fact that the optimal solution of the inner minimizing problem is $\boldsymbol{x} = 2\boldsymbol{x}^{k-1} + (t^2/2)A^{\mathrm{T}}\boldsymbol{y} - t\boldsymbol{z}$. Eliminating $\boldsymbol{z}$ from the last equation gives the following dual problem:

$$\min_{\boldsymbol{y}}\left\{-\boldsymbol{b}^{\mathrm{T}}\boldsymbol{y} + \left\|\mathrm{shrink}\left(\frac{t}{2}A^{\mathrm{T}}\boldsymbol{y} + \frac{2}{t}\boldsymbol{x}^{k-1}\right)\right\|^2 - \frac{4}{t^2}\|\boldsymbol{x}^{k-1}\|^2\right\}, \tag{3.15}$$

where

$$[\mathrm{shrink}_\mu(\boldsymbol{w})]_i = \begin{cases} w_i - \mathrm{sign}(w_i)\mu, & \text{if } |w_i| > \mu,\\ 0, & \text{otherwise,}\end{cases} \quad \forall\, \boldsymbol{w} \in \mathbb{R}^n, \quad \mu > 0$$

is the well-known shrinkage or soft-thresholding operator with parameter $\mu > 0$. We omit μ when $\mu = 1$.

Let $\boldsymbol{x}^*$ and $\boldsymbol{y}^*$ be the optimal solution to the primal problem (3.14) and the dual problem (3.15), respectively. Since strong duality holds, the optimal duality gap is zero. Moreover, (3.15) has a vanishing gradient at the optimal point $\boldsymbol{y}^*$:

$$-\boldsymbol{b} + tA\,\mathrm{shrink}\left(\frac{t}{2}A^{\mathrm{T}}\boldsymbol{y}^* + \frac{2}{t}\boldsymbol{x}^{k-1}\right) = 0.$$

Then, the optimal solution $\boldsymbol{x}^*$ of the problem (3.14) can be obtained from $\boldsymbol{y}^*$,

$$\boldsymbol{x}^* = t\,\mathrm{shrink}\left(\frac{t}{2}A^{\mathrm{T}}\boldsymbol{y}^* + \frac{2}{t}\boldsymbol{x}^{k-1}\right).$$

It is easier to obtain $\boldsymbol{x}^*$ in this way than to directly solve (3.14). In particular, there exist many efficient algorithms to solve (3.15) [27]. In this paper, we use Nesterov's accelerated gradient algorithm [30].

3.4 Choosing the parameter t

In this subsection, we prove the boundedness of the iterative points generated by Algorithm 1 solving the problem (PQA) and discuss how to appropriately choose the scaling parameter t.

Lemma 3.8. *Let $\{\boldsymbol{x}^k\}$ be the sequence generated by Algorithm* 1 *solving the problem* (PQA). *The initial point is $\boldsymbol{x}^0$ ($\boldsymbol{b} = A\boldsymbol{x}^0$). Then, for any $k \geqslant 0$, $\|\boldsymbol{x}^k\| \leqslant t/2$, where $t = \max\{2\|\boldsymbol{x}^0\|, 8\|A^{\mathrm{T}}(AA^{\mathrm{T}})^{-1}\boldsymbol{b}\|_1\}$.*

Proof. The mathematical induction is used to prove this lemma.

First, it is obvious that $\|\boldsymbol{x}^0\| \leqslant t/2$.

Second, assume that $\|\boldsymbol{x}^{k-1}\| \leqslant t/2$. We shall prove $\|\boldsymbol{x}^k\| \leqslant t/2$, where $\boldsymbol{x}^k$ is the optimal solution of

$$\min_{\boldsymbol{x}}\left\{\frac{1}{t^2}\|\boldsymbol{x} - 2\boldsymbol{x}^{k-1}\|^2 + \frac{2}{t}\|\boldsymbol{x}\|_1 : A\boldsymbol{x} = \boldsymbol{b}\right\}. \tag{3.16}$$

The dual problem of (3.16) is

$$\min_{\boldsymbol{y},\boldsymbol{z}}\left\{-\boldsymbol{b}^{\mathrm{T}}\boldsymbol{y} + \left\|\frac{t}{2}A^{\mathrm{T}}\boldsymbol{y} + \frac{2}{t}\boldsymbol{x}^{k-1} - \boldsymbol{z}\right\|^2 - \frac{4}{t^2}\|\boldsymbol{x}^{k-1}\|^2 : \|\boldsymbol{z}\|_\infty \leqslant 1\right\}. \tag{3.17}$$

Let $\boldsymbol{y}^k$ and $\boldsymbol{z}^k$ be the optimal solution of (3.17). Then

$$\boldsymbol{x}^k = 2\boldsymbol{x}^{k-1} + \frac{t^2}{2}A^{\mathrm{T}}\boldsymbol{y}^k - t\boldsymbol{z}^k, \quad \text{where} \quad \|\boldsymbol{z}^k\|_\infty \leqslant 1. \tag{3.18}$$

Multiplying (3.18) by A, we obtain ($\boldsymbol{b} = A\boldsymbol{x}^{k-1},\ \boldsymbol{b} = A\boldsymbol{x}^k$)

$$AA^{\mathrm{T}}\boldsymbol{y}^k = \frac{2}{t}A\boldsymbol{z}^k - \frac{2}{t^2}\boldsymbol{b}.$$

Since A is a matrix of full row rank, AA^{T} and $(AA^{\mathrm{T}})^{-1}$ are positive definite. Then

$$\boldsymbol{y}^k = \frac{2}{t}(AA^{\mathrm{T}})^{-1}A\boldsymbol{z}^k - \frac{2}{t^2}(AA^{\mathrm{T}})^{-1}\boldsymbol{b}. \tag{3.19}$$

Combining (3.19) and $\|\boldsymbol{z}^k\|_\infty \leqslant 1$, we have

$$\boldsymbol{b}^{\mathrm{T}}\boldsymbol{y}^k = \frac{2}{t}\boldsymbol{b}^{\mathrm{T}}(AA^{\mathrm{T}})^{-1}A\boldsymbol{z}^k - \frac{2}{t^2}\boldsymbol{b}^{\mathrm{T}}(AA^{\mathrm{T}})^{-1}\boldsymbol{b} \leqslant \frac{2}{t}\|A^{\mathrm{T}}(AA^{\mathrm{T}})^{-1}\boldsymbol{b}\|_1. \tag{3.20}$$

As $\|\boldsymbol{x}^{k-1}\| \leqslant t/2$, we can obtain $-1 \leqslant 2x_i^{k-1}/t \leqslant 1$. So

$$\left\|\mathrm{shrink}\left(\frac{2}{t}\boldsymbol{x}^{k-1}\right)\right\|^2 = 0. \tag{3.21}$$

Since $\boldsymbol{y} = 0$ is the feasible solution of (3.17), we have

$$-\boldsymbol{b}^{\mathrm{T}}\boldsymbol{y}^k + \left\|\mathrm{shrink}\left(\frac{t}{2}A^{\mathrm{T}}\boldsymbol{y}^k + \frac{2}{t}\boldsymbol{x}^{k-1}\right)\right\|^2 - \frac{4}{t^2}\|\boldsymbol{x}^{k-1}\|^2 \leqslant \left\|\mathrm{shrink}\left(\frac{2}{t}\boldsymbol{x}^{k-1}\right)\right\|^2 - \frac{4}{t^2}\|\boldsymbol{x}^{k-1}\|^2. \tag{3.22}$$

Combining (3.20)–(3.22), we have

$$\frac{1}{t^2}\|\boldsymbol{x}^k\|^2 = \left\|\mathrm{shrink}\left(\frac{t}{2}A^{\mathrm{T}}\boldsymbol{y}^k + \frac{2}{t}\boldsymbol{x}^{k-1}\right)\right\|^2 \leqslant \boldsymbol{b}^{\mathrm{T}}\boldsymbol{y}^k \leqslant \frac{2}{t}\|A^{\mathrm{T}}(AA^{\mathrm{T}})^{-1}\boldsymbol{b}\|_1.$$

Since $\|A^{\mathrm{T}}(AA^{\mathrm{T}})^{-1}\boldsymbol{b}\|_1 \leqslant t/8$, $\|\boldsymbol{x}^k\| \leqslant t/2$.

In conclusion, for any $k \geqslant 0$, $\|\boldsymbol{x}^k\| \leqslant t/2$, where $t = \max\{2\|\boldsymbol{x}^0\|, 8\|A^{\mathrm{T}}(AA^{\mathrm{T}})^{-1}\boldsymbol{b}\|_1\}$. □

By Lemma 3.8, we can obtain the following results:

1. The assumption on the boundedness of the iterative sequence $\{\boldsymbol{x}^k\}$ in Theorems 3.5 and 3.6 is satisfied. In other words, when we use Algorithm 1 to solve the problem (PQA), Algorithm 1 is convergent and the complexity bound is $\mathcal{O}(1/\epsilon)$.

2. The iterative points $\boldsymbol{x}^k,\ k \geqslant 0$ generated by (3.14) are in $[-t\boldsymbol{e}, t\boldsymbol{e}]$, when the scaling parameter $t \geqslant \max\left\{2\|\boldsymbol{x}^0\|, 8\|A^{\mathrm{T}}(AA^{\mathrm{T}})^{-1}\boldsymbol{b}\|_1\right\}$. From the proof of Lemma 3.8, we can see that there may exist a smaller t such that the iterative points $\boldsymbol{x}^k,\ k \geqslant 0$ generated by (3.14) are still in $[-t\boldsymbol{e}, t\boldsymbol{e}]$.

4 Numerical experiments

To show the effectiveness of the proposed iterative algorithm for (PQA) (the IA-PQA for short), in this section, two typical compressed sensing problems in signal recovery and image recovery are solved. For comparison, we also apply the hard algorithm [4,5], soft algorithm [13,16], FISTA [1], ALM [42] and half algorithm [38,44] to solve these problems. The performance of the algorithm is measured by how many measurements (samples) are used to recover a signal or an image. The fewer measurements required, the better the corresponding algorithm is.

The numerical experiments are carried out using MATLAB 2012(b) and running on a PC with 2.50GHZ CPU processor and 8GB RAM. The error precision is set to $\epsilon = 10^{-7}$. The iteration bound for the hard, soft and half algorithms is set to be 3,000.

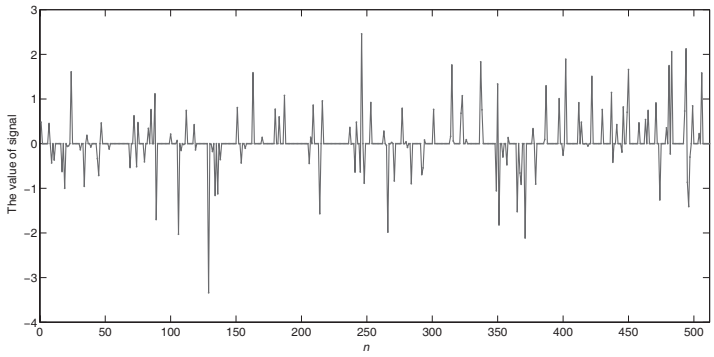

Figure 3 Sparse signal with length $n = 512$ and sparsity $k = 130$

Table 1 Recovery results of a signal with different number of samples

m	Algorithm	MSE	CPU time (s)	m	Algorithm	MSE	CPU time (s)
330	Hard	3.31E−07	0.04	270	Hard	5.61	0.06
	Soft	2.37E−04	0.47		Soft	2.62	0.18
	FISTA	4.11E−06	0.43		FISTA	2.62	0.16
	ALM	1.64E−07	0.55		ALM	2.38	1.21
	Half	4.29E−07	0.23		Half	1.01E−06	0.38
	IA-PQA	**5.98E−08**	0.14		IA-PQA	**8.54E−07**	0.33
239	Hard	6.09	0.16	238	Hard	4.86	0.12
	Soft	3.42	0.14		Soft	3.24	0.14
	FISTA	3.42	0.24		FISTA	3.24	0.26
	ALM	3.51	0.43		ALM	3.21	0.36
	Half	4.03	0.22		Half	3.00	0.27
	IA-PQA	**4.39E−07**	0.89		IA-PQA	**0.72**	1.47

4.1 Signal recovery

The signal recovery problem has been studied extensively in the past ten years [9, 17]. According to Donoho [17], the problem can be formulated as the following L_0 problem:

$$\begin{aligned} (\text{CSS}) \qquad & \min \qquad \|\boldsymbol{x}\|_0 \\ & \text{subject to} \quad \boldsymbol{b} = A\boldsymbol{x} + \boldsymbol{\varepsilon}, \end{aligned}$$

where $A \in \mathbb{R}^{m\times n}$ is a sensing matrix, $\boldsymbol{b}$ is an observation, $\boldsymbol{x}$ is the signal to be recovered, and $\boldsymbol{\varepsilon}$ is the observation noise. In this experiment, a white noise $\boldsymbol{\varepsilon} \in N(0, \sigma^2)$ ($\sigma = 0.1$) is used.

In the following, we consider two experiments (signal without noise and signal with noise) to compare the performance of L_0, L_1 and $L_{1/2}$ regularizations and the (PQA) model. In the experiments, the hard algorithm, soft algorithm, FISTA, ALM, half algorithm, and IA-PQA are tested. The sensing matrix A is taken as the Gaussian random matrix, as suggested in [17]. For each case, the mean square error (MSE) between the recovered signal and the original signal is computed, and the CPU time for all the algorithms is recorded.

4.1.1 *Signal without noise*

We consider a real-valued n-length ($n = 512$) signal $\boldsymbol{x}$ without noise, shown as in Figure 3, where $\boldsymbol{x}$ is k-sparse with $k = 130$. The experiment then aims to recover $\boldsymbol{x} \in \mathbb{R}^{512}$ through m measurements determined by $\boldsymbol{b} = A\boldsymbol{x}$, where m is much less than 512. The six algorithms are applied with a variable number (m) of measurements. Some of the numerical results are listed in Table 1.

Table 2 Recovery results of a noisy signal with different number of samples

m	Algorithm	MSE	Ratio	CPU time (s)	m	Algorithm	MSE	Ratio	CPU time (s)
	Hard	3.98	1.64	0.09		Hard	3.73	1.33	0.06
	Soft	3.73	1.54	0.08		Soft	2.90	1.04	0.09
	FISTA	3.73	1.54	0.12		FISTA	2.90	1.04	0.13
330	ALM	3.93	1.62	1.48	300	ALM	3.11	1.11	1.52
	Half	3.21	1.33	0.40		Half	2.82	1.01	0.32
	IA-PQA	3.16	**1.31**	0.85		IA-PQA	2.77	**0.99**	0.67
	Oracle	2.42				Oracle	2.80		
	Hard	4.36	1.33	0.06		Hard	6.07	1.70	0.06
	Soft	3.48	1.06	0.10		Soft	4.44	1.24	0.12
	FISTA	3.48	1.06	0.14		FISTA	4.44	1.24	0.14
280	ALM	3.60	1.10	1.39	265	ALM	4.60	1.28	1.43
	Half	2.78	**0.85**	0.61		Half	4.40	1.23	0.54
	IA-PQA	3.15	0.96	1.37		IA-PQA	4.03	**1.13**	1.79
	Oracle	3.27				Oracle	3.58		
	Hard	6.35	1.46	0.09		Hard	7.37	1.62	0.12
	Soft	4.97	1.14	0.10		Soft	5.36	1.18	0.10
	FISTA	4.97	1.14	0.12		FISTA	5.36	1.18	0.17
240	ALM	5.03	1.15	0.44	238	ALM	5.57	1.22	0.49
	Half	5.00	1.15	0.21		Half	5.94	1.30	0.26
	IA-PQA	4.74	**1.09**	0.77		IA-PQA	4.98	**1.09**	0.65
	Oracle	4.36				Oracle	4.56		

It is clear from Table 1 that all the six algorithms can accurately recover the signal when $m = 330$, and the IA-PQA attains the highest accuracy among the tested algorithms (this is true for all $m > 330$). The hard algorithm, soft algorithm, FISTA, and ALM fail to recover the signal when $m = 270$, but the half algorithm for $L_{1/2}$ regularization and the iteration algorithm for (PQA) still succeed in recovering the signal, and the IA-PQA still has the highest accuracy with a low computational cost. Furthermore, when the measurements are reduced to 239, the IA-PQA is the only one that can accurately recover the signal. When m is further reduced to 238, all the algorithms fail to recover the signal, nevertheless, the solution obtained by the IA-PQA has the highest precision.

This experiment shows that the iterative algorithm for (PQA) outperforms all the other five algorithms.

4.1.2 *Signal with noise*

Now, let us consider the case of recovering signal with noise. The signal in Figure 3 is used again, but with noise. In this experiment, we aim to assess the capability of the above six algorithms in recovering the signal from a noisy circumstance.

In order to understand the effect of noise, we use the oracle MSE to examine the recovery capability of the algorithms in the experiment. For each algorithm, we calculate the ratio between the MSE generated by the algorithm and the oracle, listed as "Ratio" in Table 2. An algorithm with a ratio closer to 1 means that it is better in terms of robustness.

The numerical results of the hard algorithm, soft algorithm, FISTA, ALM, half algorithm and IA-PQA are shown in Table 2, as the number of measurements (m) decreases from 330 to 238. We can see from Table 2 that the ratio of IA-PQA algorithm stays close to 1 regardless the value of m. Observing the MSE values in Table 2, we can find that the iterative algorithm for (PQA) always yields the most accurate recovery results. This shows that the iterative algorithm for (PQA) provides the best signal recovery at the same noise level, and yet requires the least number of samplings among the six algorithms.

4.2 Image recovery

We consider the problem of recovering realistic images, where two 256×256 pixel images and one 512×512 pixel image are selected. Each image can be denoted as an n-dimensional vector $\boldsymbol{x}$, where the dimensions are equal to 65,536, 65,536 and 262,144, respectively. The image $\boldsymbol{x}$ has a wavelet coefficient sequence $\boldsymbol{\alpha}$ that is compressible [15], where $\boldsymbol{x}=W^{\mathrm{T}}\boldsymbol{\alpha}$, and W is the discrete orthogonal wavelet transform matrix. We select the measurement matrix A as a random Fourier matrix. The experiment aims to recover the wavelet coefficient sequence $\boldsymbol{\alpha}$ through the following model:

$$\begin{aligned}(\mathrm{CSI})\qquad &\min && \|\boldsymbol{\alpha}\|_0\\ &\text{subject to} && \boldsymbol{b}=AW^{\mathrm{T}}\boldsymbol{\alpha},\end{aligned}$$

where $A\in\mathbb{R}^{m\times n}$ is a random Fourier matrix, $W\in\mathbb{R}^{n\times n}$ is a discrete orthogonal wavelet transform matrix, $\boldsymbol{b}$ is an observation and $\boldsymbol{\alpha}$ is the wavelet coefficient sequence of the image $\boldsymbol{x}$.

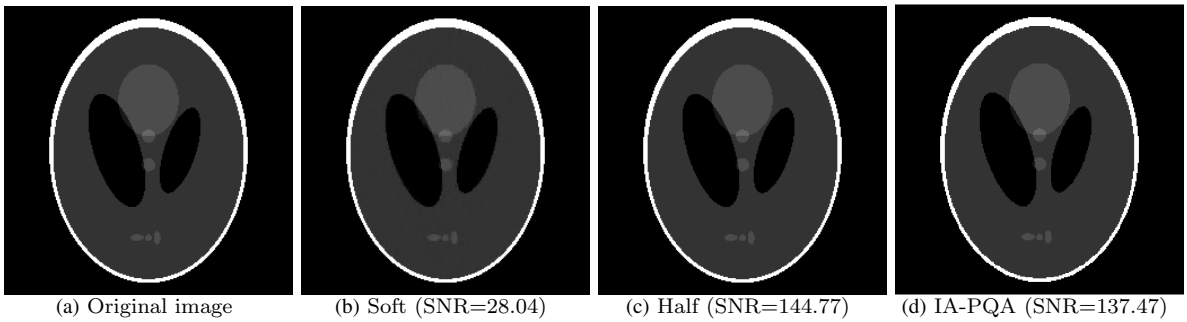

(a) Original image (b) Soft (SNR=28.04) (c) Half (SNR=144.77) (d) IA-PQA (SNR=137.47)

Figure 4 Head plantom image reconstruction results under different algorithms ($m/n=0.18$)

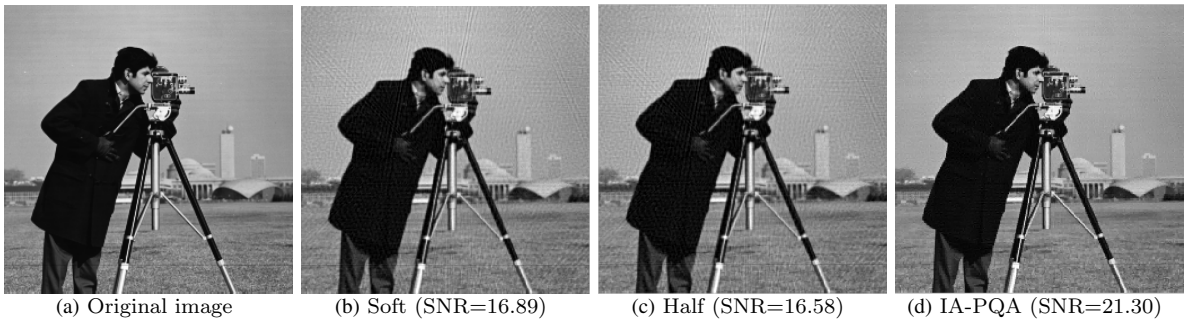

(a) Original image (b) Soft (SNR=16.89) (c) Half (SNR=16.58) (d) IA-PQA (SNR=21.30)

Figure 5 Cameraman image reconstruction results under different algorithms ($m/n=0.49$)

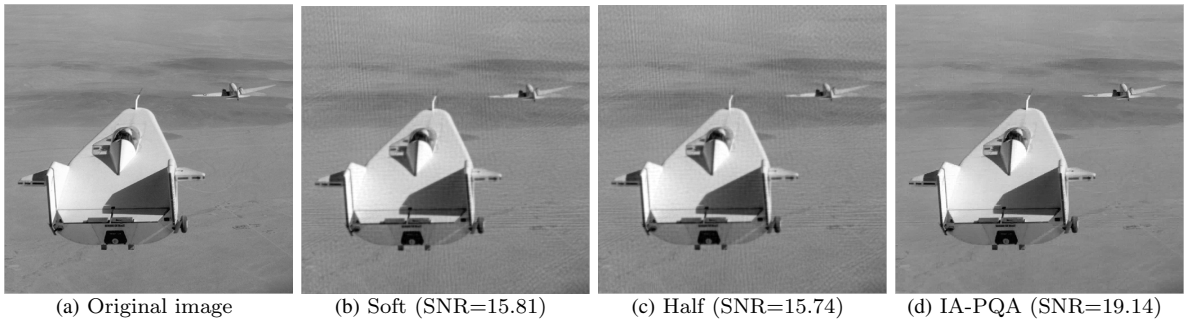

(a) Original image (b) Soft (SNR=15.81) (c) Half (SNR=15.74) (d) IA-PQA (SNR=19.14)

Figure 6 Lifting body image reconstruction results under different algorithms ($m/n=0.27$)

Table 3 Recovery results of images with different number of samples

Image	m/n	Error			SNR			CPU time (s)		
		Soft	Half	IA-PQA	Soft	Half	IA-PQA	Soft	Half	IA-PQA
Head plantom	0.39	3.29E−05	6.68E−07	1.35E−06	124.42	158.26	152.13	168.46	26.55	27.47
	0.23	0.84E−02	2.14E−06	5.65E−06	76.31	148.13	139.72	182.37	72.06	53.83
	0.18	2.17	3.15E−06	7.30E−06	28.04	144.77	137.49	229.19	122.80	89.55
Cameraman	0.74	4.21	4.82	2.10	23.52	22.34	29.57	171.42	57.38	38.78
	0.66	5.52	6.04	2.91	21.16	20.36	26.71	169.82	34.83	33.26
	0.49	9.01	9.35	5.42	16.89	16.58	21.30	193.47	16.28	35.63
Lifting body	0.44	5.95	6.06	4.77	20.59	20.43	22.51	524.49	35.82	23.76
	0.38	7.10	7.21	5.35	19.04	18.91	21.51	538.64	26.67	30.78
	0.27	10.30	10.39	7.02	15.81	15.74	19.14	537.38	16.46	40.90

We use two 256×256 images (head plantom and cameraman) and one 512×512 image (lifting body) to compare the performance of the soft algorithm, half algorithm, and IA-PQA. In each case, we compute the error $\|\boldsymbol{x} - \overline{\boldsymbol{x}}\|$, the signal to noise ratio (SNR)

$$10 \lg \frac{\|\overline{\boldsymbol{x}} - \text{mean}(\overline{\boldsymbol{x}})\|_2^2}{\|\overline{\boldsymbol{x}} - \boldsymbol{x}\|_2^2},$$

and the CPU time (s), where $\boldsymbol{x}$ is the original image and $\overline{\boldsymbol{x}}$ is the image recovered from the measurements by an algorithm. The sampling rate is measured as m/n.

Figures 4–6 illustrate visual image recovery results obtained by three algorithms, respectively. We can see from Figure 4 that when $m/n = 0.18$, the image recovery results on head plantom using the half algorithm and the IA-PQA are much better than using the soft algorithm. The result of image recovery using the IA-PQA is similar to that of the half algorithm. For the image of cameraman, when $m/n = 0.49$, the SNR of the soft and half algorithms, and IA-PQA are 16.89, 16.58, and 21.21, respectively. When $m/n = 0.27$, for the image of lifting body, the SNR of the soft and half algorithms, and IA-PQA are 15.81, 15.74, and 19.14, respectively. We note from Figures 5 and 6 that the IA-PQA can achieve the highest signal to noise ratio among the three tested algorithms.

The detailed results of image recovery under different sampling rates and different algorithms are listed in Table 3. It is clear from Table 3 that more measurements lead to a better image recovery quality. For the image of head plantom, by applying the half algorithm and the IA-PQA, both of the results can provide an accurate reconstruction of the image. For cameraman and lifting body images, the IA-PQA achieves the highest SNR among all the algorithms for different m/n. The computational time of the IA-PQA is shorter than the soft algorithm under different images and different numbers of measurements. According to Table 3, it is clear that the iterative algorithm for (PQA) outperforms the soft and the half algorithms.

5 Phase diagram research

To further show the sparsity-promoting capability of (PQA) over L_1 regularization and $L_{1/2}$ regularization, we conduct a phase transition analysis of the iterative algorithm for (PQA).

For the equivalence between L_0 and L_1 regularizations (L_1/L_0 equivalence), Donoho [17] first introduced a phase diagram to illustrate how

$$\text{sparsity} = \frac{\text{number of nonzeros in } \boldsymbol{x}}{\text{number of rows in } A} = \frac{k}{m}$$

and

$$\text{indeterminacy} = \frac{\text{number of rows in } A}{\text{number of columns in } A} = \frac{m}{n}$$

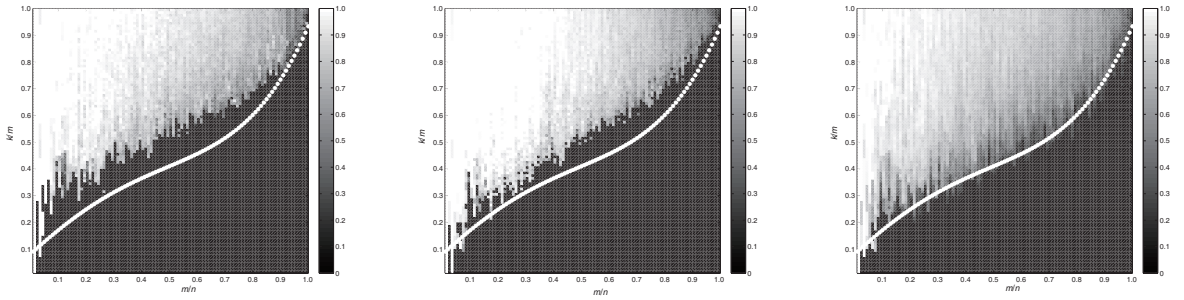

(a) IA-PQA (b) Half algorithm (c) Soft algorithm

Figure 7 Phase diagram of signal recovery using different algorithms

are related to L_1 regularization. This diagram shows a performance measure of the solution as a function of the levels of indeterminacy and sparsity. The performance of L_1 regularization exhibits a two-phase (success/failure) structure in this diagram by a phase transition curve. Above the phase transition curve, the L_1 solution is not an L_0 solution, while below the curve the L_1 solution is an L_0 solution. For this reason, the phase diagram provides a useful methodology to compare the abilities of various L_1 algorithms. We use this methodology to study the equivalence between (PQA) and L_0 regularization, and compare different approximation approaches.

We consider the 512-length signal recovery problem in Section 4 as a prototype (thus $n = 512$) with which the variable features of the problem could be constructed. More specifically, for each fixed m, we vary k from 1 to m by considering 100 equidistributed values $k_i = im/100$ ($i = 1, 2, \ldots, 100$), and then increase m from 0 to n in a way such that 100 discrete values $m_j = jn/100$ ($j = 1, 2, \ldots, 100$) are considered. This constitutes a testing situation with 10,000 models. For each model, a fixed k-sparse solution is computed by various tested algorithms. The abscissa runs from 0 to 1, and represents values for $\delta = m/n$. The ordinate is $\rho = k/m$, measuring the level of sparsity in the model.

We apply the iterative algorithm for (PQA). For comparison, we apply the soft algorithm for L_1 regularization and the half algorithm for $L_{1/2}$ regularization at the same time. The recovery is accepted as a "success" whenever the normalized root-mean-square error (nRMSE), $\|\overline{\boldsymbol{x}} - \boldsymbol{x}\|/\|\boldsymbol{x}\|$, is smaller than 10^{-5}; otherwise, it is regarded as a "failure", where $\boldsymbol{x}$ is the original signal and $\overline{\boldsymbol{x}}$ is the signal recovered from the fewer measurements. The dark black area indicates where the point is the case of "success", but the other area indicates "failure". In this way, the phase diagram of each algorithm is shown below.

Figure 7 shows the phase diagrams of the IA-PQA, half, and soft algorithms, respectively. The commonly appearing dashed curves are the phase transition curves of L_1 regularization, which consists of the theoretical thresholds at which L_1/L_0 equivalence breaks down.

We can see from Figure 7 that the phase transition phenomenon does appear for all the algorithms. The phase diagram of the soft algorithm almost coincides with the theoretical one. It is very pleasing to observe that the phase diagrams of the IA-PQA and half algorithm in Figures 7(a) and 7(b) show that the phase transition curves are all above the L_1 curve. As expected, it shows the stronger sparsity-promoting property of (PQA) and $L_{1/2}$ regularization over L_1 regularization. Moreover, the performance of (PQA) is superior to $L_{1/2}$ regularization over $[0, 0.7]$, at least as well as $L_{1/2}$ regularization over $[0.7, 1]$.

6 Conclusions

In this paper, we have proposed a new piecewise quadratic approximation framework for solving sparsity problems. The main contributions are the establishment of a piecewise quadratic approximation model, and the iterative algorithm for (PQA).

Numerical experiments have shown that (PQA) can get the best sparse solutions of a problem and recover a signal or an image from the fewest samplings, as compared with L_1 and $L_{1/2}$ regularizations,

and the iterative algorithm is fast and effective for solving (PQA). In addition, we have conducted a phase diagram analysis to further show the superiority of (PQA) over L_1 and $L_{1/2}$ regularizations.

Acknowledgements This work was supported by National Natural Science Foundation of China (Grant No. 11771275).

References

1 Beck A, Teboulle M. A fast iterative shrinkage-thresholding algorithm for linear inverse problems. SIAM J Imaging Sci, 2009, 2: 183–202
2 Becker S, Bobin J, Cands E J. NESTA: A fast and accurate first-order method for sparse recovery. SIAM J Imaging Sci, 2011, 4: 1–39
3 Bioucas-Dias J M, Figueiredo M A. A new TwIST: Two-step iterative shrinkage/thresholding algorithms for image restoration. IEEE Trans Image Process, 2007, 16: 2992–3004
4 Blumensath T, Davies M E. Iterative thresholding for sparse approximations. J Fourier Anal Appl, 2008, 14: 629–654
5 Blumensath T, Davies M E. Iterative hard thresholding for compressed sensing. Appl Comput Harmon Anal, 2008, 27: 265–274
6 Bredies K, Lorenz D A, Reiterer S. Minimization of non-smooth, non-convex functionals by iterative thresholding. J Optim Theory Appl, 2014, 165: 78–112
7 Bruckstein A M, Donoho D L, Elad M. From sparse solutions of systems of equations to sparse modeling of signals and images. SIAM Rev, 2009, 51: 34–81
8 Candes E J, Recht B. Exact matrix completion via convex optimization. Found Comput Math, 2008, 9: 717–772
9 Candes E J, Romberg J, Tao T. Robust uncertainty principles: Exact signal reconstruction from highly incomplete frequency information. IEEE Trans Inform Theory, 2006, 52: 489–509
10 Candes E J, Wakin M B, Boyd S P. Enhancing sparsity by reweighted l_1 minimization. J Fourier Anal Appl, 2008, 14: 877–905
11 Cao W F, Sun J, Xu Z B. Fast image deconvolution using closed-form thresholding formulas of L_q $(q = 1/2, 2/3)$ regularization. J Vis Comm Image Represent, 2013, 24: 1529–1542
12 Chen S S, Donoho D L, Saunders M A. Atomic decomposition by basis pursuit. SIAM J Sci Comput, 1998, 20: 33–61
13 Daubechies I, Defrise M, Christine D M. An iterative thresholding algorithm for linear inverse problems with a sparsity constraint. Comm Pure Appl Math, 2004, 57: 1413–1457
14 Daubechies I, Devore R, Fornasier M, et al. Iteratively reweighted least squares minimization for sparse recovery. Comm Pure Appl Math, 2010, 63: 1–38
15 Devore R, Jawerth B. Image compression through wavelet transform coding. IEEE Trans Inform Theory, 1992, 38: 719–746
16 Donoho D L. De-noising by soft-thresholding. IEEE Trans Inform Theory, 1995, 41: 613–627
17 Donoho D L. Compressed sensing. IEEE Trans Inform Theory, 2006, 52: 1289–1306
18 Efron B, Hastie T. Least angle regression. Ann Statist, 2004, 32: 407–499
19 Fan J, Li R. Variable selection via nonconcave penalized likelihood and its oracle properties. J Amer Statist Assoc, 2001, 96: 1348–1360
20 Gasso G, Rakotomamonjy A, Canu S. Recovering sparse signals with a certain family of non-convex penalties and DC programming. IEEE Trans Signal Process, 2009, 57: 4686–4698
21 Geman D, Reynolds G. Constrained restoration and the recovery of discontinuities. IEEE Trans Pattern Anal Mach Intell, 1992, 14: 367–383
22 Geman D, Yang C. Nonlinear image recovery with half-quadratic regularization. IEEE Trans Image Process, 1995, 4: 932–946
23 Gong P H, Zhang C S, Lu Z S, et al. A general iteartive shrinkage and thresholding algorithm for non-convex regularized optimization problems. Proc Int Conf Mach Learn, 2013, 28: 37–45
24 Gorodnitsky I F, Rao B D. Sparse signal reconstruction from limited data using FOCUSS: A re-weighted minimum norm algorithm. IEEE Trans Signal Process, 1997, 45: 600–616
25 Hale E T, Yin W, Zhang Y. A fixed-point continuation method for L_1-minimization: Methodology and convergence. SIAM J Optim, 2008, 19: 1107–1130
26 Lai M J, Xu Y Y, Yin W T. Improved iteratively reweighted least squares for unconstrained smoothed L_q minimization. SIAM J Numer Anal, 2013, 51: 927–957
27 Lai M J, Yin W T. Augmented L_1 and nuclear-norm models with a globally linearly convergent algorithm. SIAM J Imaging Sci, 2013, 6: 1059–1091
28 Moreau J J. Proximite et dualite dans un espace hilbertien. Bull Soc Math France, 1965, 93: 273–299
29 Natarajan B K. Sparse approximate solutions to linear systems. SIAM J Comput, 1995, 24: 227–234

30 Nesterov Y. Introductory Lectures on Convex Optimization: A Basic Course. Boston: Springer, 2003
31 Parikh N, Boyd S. Proximal algorithms. Found Trends Optim, 2013, 1: 123–231
32 Qian Y T, Jia S, Zhou J, et al. Hyperspectral unmixing via sparsity-constrained nonnegative matrix factorization. IEEE Trans Geosci Remote Sens, 2011, 49: 4282–4297
33 Rakotomamonjy A, Flamary R, Gasso G, et al. L_p-L_q penalty for sparse linear and sparse multiple kernel multitask learning. IEEE Trans Neural Netw, 2011, 22: 1307–1320
34 Tibshirani R. Regression shrinkage and selection via the LASSO. J R Stat Soc Ser B, 1996, 58: 267–288
35 Wen B, Chen X J, Pong T K. Linear convergence of proximal gradient algorithm with extrapolation for a class of nonconvex nonsmooth minimizaiton porblems. SIAM J Optimi, 2017, 27: 124–145
36 Wu B. High-dimensional analysis on matrix decomposition with applications to correlation matrix estimation in factor models. PhD Thesis. Singapore: National University of Singapore, 2014
37 Xu Z B. Data modeling: Visual psychology approach and $L_{1/2}$ regularization theory. In: Proceedings of the International Congress of Mathematicians. Berlin: International Mathematical Union, 2010, 3151–3184
38 Xu Z B, Chang X Y, Xu F M, et al. $L_{1/2}$ regularization: A thresholding representation theory and a fast solver. IEEE Trans Neural Netw Learn Syst, 2012, 23: 1013–1027
39 Xu Z B, Guo H L, Wang Y, et al. Representative of $L_{1/2}$ regularization among L_q $(0 < q < 1)$ regularizations: An experimental study based on phase diagram. Acta Automat Sinica, 2012, 38: 1225–1228
40 Xu Z B, Zhang H, Wang Y, et al. $L_{1/2}$ regularization. Sci China Inf Sci, 2010, 53: 1159–1169
41 Yang A Y, Ganesh A, Ma Y. Robust face recognition via sparse representation. IEEE Trans Pattern Anal Mach Intell, 2009, 31: 210–227
42 Yang A Y, Ganesh A, Zhou Z H, et al. Fast L_1-minimization algorithms for robust face recognition. IEEE Trans Image Process, 2013, 22: 3234–3246
43 Yin P H, Lou Y F, He Q, et al. Minimization of L_{1-2} for compressed sensing. SIAM J Sci Comput, 2015, 37: 536–563
44 Zeng J S, Lin S B, Wang Y, et al. $L_{1/2}$ regularization: Convergence of iterative half thresholding algorithm. IEEE Trans Signal Process, 2014, 62: 2317–2329
45 Zeng J S, Lin S B, Xu Z B. Sparse regularization: Convergence of iterative jumping thresholding algorithm. IEEE Trans Signal Process, 2014, 64: 5106–5118
46 Zhang C H. Nearly unbiaised variable selection under minimax concave penalty. Ann Statist, 2010, 38: 894–942
47 Zhang T. Analysis of multi-stage convex relaxation for sparse regularization. J Mach Learn Res, 2010, 11: 1081–1107